

## Dual superconductivity and vacuum properties in Yang–Mills theories

A. D’Alessandro<sup>a</sup>, M. D’Elia<sup>a</sup> and L. Tagliacozzo<sup>b</sup> \*

<sup>a</sup>*Dipartimento di Fisica, Università di Genova and INFN, Sezione di Genova,  
 Via Dodecaneso 33, I-16146 Genova, Italy*

<sup>b</sup>*Departament d’Estructura i Constituents de la Matèria, Universitat de Barcelona,  
 647, Diagonal, 08028, Barcelona, Spain.*

### Abstract

We address, within the dual superconductivity model for color confinement, the question whether the Yang–Mills vacuum behaves as a superconductor of type I or type II. In order to do that we compare, for the theory with gauge group  $SU(2)$ , the determination of the field penetration depth  $\lambda$  with that of the superconductor correlation length  $\xi$ . The latter is obtained by measuring the temporal correlator of a disorder parameter developed by the Pisa group to detect dual superconductivity. The comparison places the vacuum close to the border between type I and type II and marginally on the type II side. We also check our results against the study of directly measurable effects such as the interaction between two parallel flux tubes, obtaining consistent indications for a weak repulsive behaviour. Future strategies to improve our investigation are discussed.

### I. INTRODUCTION

Color confinement emerges as a fundamental property of strongly interacting matter from experimental facts, like for instance the absence of fractionally charged particles. Even if lattice simulations provide evidence that confinement is realized in the theory of strong interactions, a full theoretical explanation of it starting from QCD first principles is still lacking. However models exist which relate confinement to some property of the fundamental state of the theory. One of those models is based on dual superconductivity of the QCD vacuum [1–3]: according to this model confinement of color is due to the spontaneous breaking of a magnetic symmetry which yields a nonvanishing magnetically charged Higgs condensate. The dual Meissner effect compels the electric field between static colored charges in narrow flux tubes, giving rise to a linearly rising potential and to confinement. The broken magnetic group is chosen by a procedure known as *Abelian projection* [4]: a local operator  $\phi(x)$  transforming in the adjoint representation is diagonalized, leaving a residual  $U(1)^{N_c-1}$  gauge symmetry.

---

\*E-mail addresses: adales@ge.infn.it, delia@ge.infn.it, luca@ecm.ub.es

A superconductor is characterized by two fundamental parameters, the correlation length  $\xi$  of the Higgs condensate and the field penetration depth  $\lambda$ : they determine whether the superconductor is of type I ( $\xi > \lambda$ ) or type II ( $\xi < \lambda$ ). In a superconductor of type I an external field  $B$  is always expelled from the medium till a critical value  $B_c$  beyond which superconductivity disappears. In a superconductor of type II there are instead two different critical values  $B_{c1}$  and  $B_{c2}$ , and for  $B_{c1} < B < B_{c2}$  the external field can penetrate the medium in the form of Abrikosov flux tubes, without disrupting superconductivity. Another relevant property of type II superconductors is the repulsive interaction between two parallel flux tubes, which is instead attractive for type I superconductors.

In the framework of the dual superconductor model, understanding whether the QCD vacuum behaves as a type I or a type II superconductor is an issue which can help clarifying the dynamics of color confinement and of flux tube interactions. The question can in principle be answered by QCD numerical lattice simulations and several efforts have been done in the past in that direction, mostly for the pure gauge theory with 2 colors. A direct way to determine  $\lambda$  is a lattice analysis [5–10] of the flux tube which is formed between two static color charges: the longitudinal (chromo)electric field  $E_z$  decays asymptotically as  $E_z = AK_0(\frac{d}{\lambda})$  at a radial distance  $d$  from the tube axis.

The determination of  $\xi$  is less straightforward: this parameter has been found in literature mostly either through an analysis of violations of the  $E_z = AK_0(\frac{d}{\lambda})$  behavior close to the center of the flux tube [6,10] or through some global fit to the whole set of Ginzburg-Landau equations [7–9]; a determination based on a direct analysis of the condensate distribution around the flux tube has also appeared recently [11]. An approximate picture has emerged placing the  $SU(2)$  Yang-Mills vacuum roughly at the boundary between a type I and a type II dual superconductor.

In the present study we consider the case of  $SU(2)$  pure gauge theory and follow a different strategy, aimed at determining the mass of the Higgs field  $m_H = 1/\xi$  through the analysis of the temporal correlator of an observable directly coupled to it: that is the operator  $\mu$  developed by the Pisa group which creates a magnetic monopole (see Ref. [12] for a detailed discussion about its definition and also Ref. [13] and [14] for related parameters). Its vacuum expectation value (*v.e.v.*)  $\langle\mu\rangle$  is a good disorder parameter detecting dual superconductivity ( $\langle\mu\rangle \neq 0$ ) and the transition to the deconfined - normal conducting phase ( $\langle\mu\rangle = 0$ ) both in pure gauge theory [15–17] and in full QCD [18,19]. We will compare results obtained for  $\xi$  in this way with those obtained for  $\lambda$  through the usual analysis of the field inside the flux tube. As a further independent method to characterize the QCD vacuum, we will also directly study the interaction between flux tubes by measuring the electric field in presence of two couples of static charges. Preliminary results concerning the determination of  $\xi$  have been reported in Ref. [20].

In Section II we will review the definition of the disorder parameter  $\langle\mu\rangle$  and present a determination of  $\xi$  based on the measurement of its temporal correlator. The results obtained for  $\xi$  will be compared in Section III with those obtained for  $\lambda$ . Conclusions concerning the typology of the vacuum will then be checked against a direct analysis of flux tube interactions in Section IV. Finally in Section V we will present our conclusions and discuss possible improvements as well as possible future extensions of our study.

## II. DISORDER PARAMETER FOR DUAL SUPERCONDUCTIVITY AND DETERMINATION OF THE CORRELATION LENGTH $\xi$

### A. The disorder parameter and its temporal correlator

A disorder parameter detecting dual superconductivity can be constructed in terms of an operator  $\mu$  which creates a magnetic charge. It can be defined in the continuum as [12]:

$$\mu^a(\vec{x}, t) = \exp \left( i \int d\vec{y} \text{Tr} \{ \phi^a(\vec{y}, t) \vec{E}(\vec{y}, t) \} \vec{b}_\perp(\vec{y} - \vec{x}) \right) \quad (2.1)$$

where  $\phi^a(\vec{y}, t)$  is the adjoint field defining the abelian projection,  $\vec{b}_\perp$  is the field of a monopole sitting at  $\vec{x}$  and  $\vec{E}(\vec{y}, t)$  is the chromoelectric field. The construction of  $\mu$  is analogous to that of a translational operator in quantum mechanics: it creates a magnetic monopole by shifting the quantum vector potential field by the classical field  $\vec{b}_\perp$ . On the lattice correlation functions of  $\mu(\vec{x}, t)$  can be written as (see [12,15–17] for details):

$$\langle \bar{\mu}(t', \vec{x}') \mu(t, \vec{x}) \rangle = \frac{\tilde{Z}}{Z} = \frac{\int (\mathcal{D}U) e^{-\beta \tilde{S}}}{\int (\mathcal{D}U) e^{-\beta S}} \quad (2.2)$$

where  $S$  is the usual pure gauge action and  $\tilde{S}$  differs from  $S$  only at time slices  $t$  and  $t'$ . In particular, in the abelian projected gauge the temporal plaquettes

$$\Pi_{i0}(\vec{y}, y_0) = U_i(\vec{y}, y_0) U_0(\vec{y} + \hat{i}, y_0) U_i^\dagger(\vec{y}, y_0 + \hat{0}) U_0^\dagger(\vec{y}, y_0) \quad (2.3)$$

are changed by substituting

$$U_i(\vec{y}, y_0) \rightarrow \tilde{U}_i(\vec{y}, y_0) \equiv U_i(\vec{y}, y_0) e^{iTb_\perp^i(\vec{y}-\vec{x})} \quad (2.4)$$

where  $T$  is the diagonal gauge group generator corresponding to the monopole species chosen ( $T_3 = \lambda_3/2$  is the only possible choice for the  $SU(2)$  gauge group) and  $b_\perp^i$  is the transverse vector field corresponding to the monopole (antimonopole) sitting at  $t$  ( $t'$ ) and  $\vec{x}$ .

The numerical study of the temporal correlator of  $\mu$  as a mean to determine the monopole mass has already been considered for the  $U(1)$  pure gauge theory in 4 dimensions [12,21]. In the confined phase, where dual superconductivity is at work,  $\langle \mu \rangle \neq 0$ . Therefore at large temporal distances the correlator  $\langle \bar{\mu}(t, \vec{x}) \mu(0, \vec{x}) \rangle$  is dominated, by cluster property, by a term  $\langle \mu \rangle^2$  plus a function which vanishes exponentially according to the mass  $M$  of the lightest state coupled to  $\mu$ . Taking into account that we are computing a point-point correlator instead of a zero momentum one and neglecting the possible presence of excited states, we will consider as the simplest possible ansatz the leading large distance behaviour of the two point correlation function:

$$\langle \bar{\mu}(t, \vec{x}) \mu(0, \vec{x}) \rangle \simeq \langle \mu \rangle^2 + \gamma \frac{e^{-Mt}}{t^{3/2}}. \quad (2.5)$$

Since the ratio of partition functions in Eq. (2.2) is an exponentially noisy quantity, it is not easy to measure the correlator  $\langle \bar{\mu} \mu \rangle$  directly and one usually measures:

$$\rho = \frac{d}{d\beta} \ln \langle \bar{\mu} \mu \rangle = \langle S \rangle_S - \langle \tilde{S} \rangle_{\tilde{S}} \quad (2.6)$$

where the subscript indicates the action that is used in the Boltzmann weight. The behaviour expected for  $\rho$  at large  $t$  can be easily derived from Eq. (2.5); after introducing the adimensional lattice quantities  $\hat{M} = aM$ ,  $\hat{t} = t/a$ ,  $\vec{n} = \vec{x}/a$  and after rescaling  $\gamma \rightarrow a^{\frac{3}{2}}\gamma$ , where  $a$  is the lattice spacing, one obtains:

$$\rho(\hat{t}) \equiv \frac{d}{d\beta} \ln \langle \bar{\mu}(\hat{t}, \vec{n}) \mu(0, \vec{n}) \rangle \simeq \frac{A + B e^{-\hat{M}\hat{t}} / \hat{t}^{1/2} + C e^{-\hat{M}\hat{t}} / \hat{t}^{3/2}}{\langle \mu \rangle^2 + \gamma e^{-\hat{M}\hat{t}} / \hat{t}^{3/2}} \quad (2.7)$$

where

$$A = \frac{d\langle \mu \rangle^2}{d\beta}; \quad B = -\gamma \frac{d\hat{M}}{d\beta} = -\gamma M \frac{da}{d\beta}; \quad C = \frac{d\gamma}{d\beta}. \quad (2.8)$$

Eq. (2.7) will be the basis for our fits to the temporal correlator  $\rho(\hat{t})$ , which will be discussed in Section II B. Results obtained through a different observable, also related to the temporal correlator in Eq. (2.5) and introduced in Ref. [21], will be presented and discussed in Section II D.

As a result of our fits we will obtain an estimate of  $\xi_\mu \equiv a\hat{M}^{-1}$ . The fact that  $\langle \mu \rangle$  is a good disorder parameter for dual superconductivity means that it is surely coupled to the condensing Higgs field. The natural expectation is therefore that  $\xi_\mu = \xi$ , which is true apart from the unlikely case where the actual field which condenses in the vacuum does not coincide with the lowest mass state having the same quantum numbers (in that case one would have  $\xi < \xi_\mu$ ).

## B. Monte Carlo simulations and discussion of results

We have measured the correlator  $\rho(\hat{t})$  using a magnetic charge defined in the so-called random abelian projection, which was proposed in Ref. [17] and is a sort of average over all possible abelian projections: in that case one thus does not need to perform any gauge fixing at all, with a great benefit in computational cost. The dependence of our results on the abelian projection chosen will be discussed in Section II C, where we will make a comparison with results obtained by taking the abelian projection in the gauge where the Polyakov loop is diagonal.

The correlator  $\rho(\hat{t})$  is composed of two terms (see Eq. (2.6)):

$$\rho(\hat{t}) = \langle S \rangle_S - \langle \tilde{S}(\hat{t}) \rangle_{\tilde{S}(\hat{t})}; \quad (2.9)$$

since the first term is independent of  $\hat{t}$ , we have only determined the expectation value of the modified action  $\langle \tilde{S}(\hat{t}) \rangle_{\tilde{S}(\hat{t})}$ : we notice that a different Monte Carlo simulation is required for each value of  $\hat{t}$ .

We have performed simulations at four different values of the inverse bare coupling,  $\beta = 2.4, 2.5115, 2.6, 2.7$ , in order to eventually check the correct scaling of our results to the continuum limit. For the determination of the physical scale we make reference to

the non-perturbative computation of the  $\beta$ -function and to the determination of  $T_c/\sqrt{\sigma}$  reported in Refs. [22,23], from which we have inferred the following values of the lattice spacing:  $a(\beta = 2.4) \simeq 0.118$  fm,  $a(\beta = 2.5115) \simeq 0.083$  fm,  $a(\beta = 2.6) \simeq 0.062$  fm and  $a(\beta = 2.7) \simeq 0.046$  fm. The lattice volumes  $N_s^3 \times N_t$  have been chosen so as to have approximately equal spatial volumes at the three lowest coupling values:  $12^3 \times 16$  at  $\beta = 2.4$ ,  $16^3 \times 20$  at  $\beta = 2.5115$ ,  $20^3 \times 20$  at  $\beta = 2.6$ . At  $\beta = 2.7$  we have been compelled by computational constraints to use again a  $20^3 \times 20$  lattice, which is smaller in physical units, but is however comparable, as for the spatial size, to a  $12^3 \times 20$  lattice at  $\beta = 2.5115$ , where we have checked that finite size effects in the determination of  $\xi$  are negligible, at least within our statistical uncertainties. Different values of the magnetic charge  $Q$  carried by the monopole have been used in some cases, in order to check that our results are independent of this quantity.

The signal obtained for  $\langle \tilde{S}(\hat{t}) \rangle_{\tilde{S}(\hat{t})}$  is mostly made up of a constant background: it is therefore essential to reduce the noise as much as possible to obtain a good definition of the exponentially decaying signal. In order to do that we have integrated analytically over the probability measure of each gauge link (as the other links were left fixed), thus obtaining an improved estimate for the local action density. The typical number of measurements taken for each determination of the temporal correlator has ranged from  $10^6$  to about  $5 \cdot 10^6$ . We report in Fig. 1 a summary of the results obtained for the modified action density  $\tilde{\Pi}(\hat{t}) \equiv \langle \tilde{S}(\hat{t}) \rangle_{\tilde{S}(\hat{t})}/6V$ .

The expected behaviour for  $\tilde{\Pi}(\hat{t})$  stems from Eq. (2.7) by simply adding a constant term; as a matter of fact, due to the high number of parameters in Eq. (2.7) and to the poor quality of our signal, we have been able to fit only the leading large  $\hat{t}$  behaviour of Eq. (2.7),<sup>†</sup> which taking into account the periodic boundary conditions in the time direction is

$$\tilde{\Pi}(\hat{t}) = A' + B' \left( \frac{e^{-\hat{t}/\hat{\xi}}}{\hat{t}^{1/2}} + \frac{e^{-(N_t - \hat{t})/\hat{\xi}}}{(N_t - \hat{t})^{1/2}} \right) \quad (2.10)$$

In Table I we report the fit results obtained for  $\hat{\xi}$  according to Eq. (2.10) as a function of the initial fitting point  $\hat{t}_0$ : since we are taking into account only the leading large  $\hat{t}$  behaviour, and also in order to avoid contaminations from higher excited states coupled to  $\mu$ , we must search for a plateau in  $\hat{\xi}$  as a function of  $\hat{t}_0$ . That is not an easy task since, as we will soon discuss, the correlation length  $\xi$  comes out to be of the order of 0.1 fm: that, combined with the very low signal/noise ratio characterizing our observable, leads to a signal which disappears after a few lattice spacings, so that fits for  $\hat{t}_0 \geq 4$  are hardly feasible, except for the highest values of  $\beta$  and  $Q$  where  $\hat{\xi}$  is larger and the signal sharper.

As a general rule, we have considered for our determination of  $\hat{\xi}$  the value of  $\hat{t}_0$  after which the signal does not change considerably within errors: that corresponds to  $\hat{t}_0 = 2$  for  $\beta = 2.4$ ,  $\hat{t}_0 = 3$  for  $\beta = 2.5115$  and  $\beta = 2.6$ ,  $\hat{t}_0 = 4$  for  $\beta = 2.7$ . The corresponding values obtained for the  $\tilde{\chi}^2$  test are the following:  $\chi^2/\text{d.o.f.}(12^3 \times 16, \beta = 2.4) = 0.46/3$ ,  $\chi^2/\text{d.o.f.}(12^3 \times 20, \beta = 2.5115) = 1.2/2$ ,  $\chi^2/\text{d.o.f.}(16^3 \times 20, \beta = 2.5115) = 2.1/5$ ,  $\chi^2/\text{d.o.f.}(20^3 \times 20, \beta = 2.6, Q =$

---

<sup>†</sup>A fit which takes into account also the next to leading term,  $e^{-\hat{t}/\hat{\xi}}/\hat{t}^{3/2}$ , gives compatible results, but errors are of the same order of the fitted values.

2) = 2.7/3,  $\chi^2/\text{d.o.f.}(20^3 \times 20, \beta = 2.6, Q = 8) = 1.3/3$  and  $\chi^2/\text{d.o.f.}(20^3 \times 20, \beta = 2.7) = 6.4/4$ . The two determinations obtained at  $\beta = 2.5115$  on the two different lattice sizes are in agreement, thus indicating that finite size effects are not important within our present statistical errors. The two determinations obtained at  $\beta = 2.6$  for two different values of the monopole charge are nicely compatible within errors, thus showing no significant dependence of  $\xi$  on  $Q$ .

For the two lowest values of  $\beta$  the resulting value of  $\xi$  is quite close, actually compatible, with the value of the lattice spacing itself, so that lattice artifacts could play an important role. The situation improves for  $\beta = 2.6$  and  $\beta = 2.7$ , which can then be considered as more reliable determinations: we notice that the two values  $\hat{t}_0 = 3$  and  $\hat{t}_0 = 4$  used respectively for the determinations at  $\beta = 2.6$  and  $\beta = 2.7$  are approximately equal when converted in physical units.

In Table II we report a summary of the values in physical units obtained for  $\xi$  as a function of  $\beta$ , together with the lattice spacing  $a(\beta)$ . Our results seem compatible, within errors, with the correct scaling to the continuum limit; however, taking into account that the determinations at the two lowest values of  $\beta$  are very close to the ultraviolet cutoff and that in general our statistical uncertainties are still large, a reliable extrapolation to the continuum limit is still not possible. Rather we give as our best determination of the correlation length  $\xi$  that obtained at  $\beta = 2.7$ , which, using a conservative estimate for the error, is  $\xi = 0.11 \pm 0.02$  fm. We will come back to these results in Section III where we will compare them with those obtained for the dual penetration length  $\lambda$ .

### C. Independence of the abelian projection

In the present Section we will discuss the possible dependence of  $\xi$  on the abelian projection chosen to define  $\mu$ . The natural physical expectation is that  $\xi$  be an universal quantity characterizing the Yang-Mills vacuum, hence independent of the particular abelian projection chosen. This is consistent with 't Hooft ansatz that all abelian projections are equivalent to each other: that equivalence also emerges from numerical determinations of  $\langle \mu \rangle$ , which have clearly showed that  $\langle \mu \rangle$  being zero or non zero is a gauge independent statement [15–17]. A possible theoretical argument is the following: the operator  $\mu$  defined in one particular abelian projection creates a magnetic charge in every other abelian projection [19,24]; this implies that the lowest mass state coupled to  $\mu$  should be universal, *i.e.*  $\xi$  should be independent of the abelian projection chosen. In order to test that hypothesis we have repeated our measurements for the abelian projection defined by diagonalizing  $P(\vec{n}, \hat{t})$  on each lattice site, where  $P(\vec{n}, \hat{t})$  is the Polyakov loop at the spatial site  $\vec{n}$  starting at time  $\hat{t}$ .

The updating procedure in this case is not as simple as in the case of the random abelian projection: changes in Polyakov loops modify the abelian projection and as a consequence also the modified action  $\tilde{S}$ , which therefore is not a linear function of the temporal links. On those links usual heat-bath or over-relaxation updatings are not possible and we have used a metropolis algorithm. Numerical strategies for noise reduction like link integration are no more feasible and as a consequence there is a considerable increase in computational effort with respect to the case of the random abelian projection.

We have performed a numerical simulation in the Polyakov gauge at  $\beta = 2.4$  on a  $12^3 \times 20$  lattice. The results obtained in this case show a good agreement with the determination in

the random gauge, as can be appreciated from Fig. 2. A fit according to Eq. (2.10) gives  $\hat{\xi}(\beta = 2.4) = 1.3 \pm 0.8$ , which is in agreement, even if within the large errors, with the value obtained in the random gauge.

#### D. Comparison with a different approach

An alternative way to study the temporal correlator of the disorder parameter, inspired by studies in gaugeball spectroscopy [25], has been introduced for the  $U(1)$  pure gauge theory in Ref. [21], and consists in considering a new observable  $\tilde{\rho}$ , which is the derivative of  $\ln\langle\bar{\mu}(\hat{t}, \vec{n})\mu(0, \vec{n})\rangle$  with respect to the adimensional temporal distance  $\hat{t}$  in place of the inverse gauge coupling  $\beta$ . The expected behaviour for  $\tilde{\rho}$  can be easily derived from Eq. (2.5)

$$\tilde{\rho}(\hat{t}) \equiv \frac{d}{d\hat{t}} \ln\langle\bar{\mu}(\hat{t}, \vec{n})\mu(0, \vec{n})\rangle \simeq - \left( \hat{M} + \frac{3}{2\hat{t}} \right) \frac{\gamma e^{-\hat{M}\hat{t}/\hat{t}^{3/2}}}{\langle\mu\rangle^2 + \gamma e^{-\hat{M}\hat{t}/\hat{t}^{3/2}}}. \quad (2.11)$$

Two features of the new observable  $\tilde{\rho}$  are apparent from Eq. (2.11): 1) the disconnected large distance contribution has disappeared in taking the derivative, so that  $\tilde{\rho}$  takes into account only the interesting connected piece without any noisy background; 2) there are only 3 parameters ( $\hat{M}$ ,  $\gamma$  and  $\langle\mu\rangle^2$ ) to be fitted. Both things could contribute to make  $\tilde{\rho}$  a better observable than  $\rho$  in order to extract the correlation length  $\hat{\xi} = \hat{M}^{-1}$ . To test that possibility and to have an independent check of the results presented in Section II B, we have repeated our determination of  $\xi$  by measuring the correlator  $\tilde{\rho}(\hat{t})$ .

A drawback of  $\tilde{\rho}$  is that its definition on the lattice requires a prescription for the discretized derivative, implying the possible presence of further systematic effects due to the finite lattice spacing. Let us rewrite the  $\langle\bar{\mu}\mu\rangle$  correlator in the form

$$\langle\bar{\mu}(\hat{t})\mu(0)\rangle = \frac{\int (\mathcal{D}U) e^{-\beta(S+\Delta S_0+\Delta S_{\hat{t}})}}{\int (\mathcal{D}U) e^{-\beta S}}, \quad (2.12)$$

where  $\Delta S_0$  and  $\Delta S_{\hat{t}}$  indicate the changes in the action in correspondence of the monopole creation and destruction operators respectively; we will define  $\tilde{\rho}$  by taking the symmetric derivative, which can be written as (see Ref. [21] for details):

$$\tilde{\rho}(\hat{t}) = -\frac{\beta}{2} \left\langle (\Delta S_{\hat{t}+1} - \Delta S_{\hat{t}-1}) \right\rangle_{S+\Delta S_0+\Delta S_{\hat{t}}} \quad (2.13)$$

We have performed our measurement at  $\beta = 2.5115$  on a lattice  $12^3 \times 16$ . Our results are reported in Fig. 3 together with the best fit result obtained using Eq. (2.11) after taking into account the periodic boundary conditions in the time direction<sup>‡</sup>: the first point included in the fit has been  $\hat{t}_0 = 3$ . We have obtained  $\hat{\xi} = 1.32(25)$  ( $\xi = 0.110(21)$  fm in physical units) with  $\chi^2/\text{d.o.f.} = 1.8/3$ . We conclude that the agreement with the results obtained by measuring  $\rho$  is very good (see Tables I and II): this consistency gives an indication that

---

<sup>‡</sup>Since  $\tilde{\rho}(\hat{t})$  is the first derivative of the temporal correlator, it is an odd function with respect to  $\hat{t} = N_t/2$ , as is clearly verified from Fig. 3.

systematic effects in the determination of  $\xi$  are under control both when  $\rho$  or  $\tilde{\rho}$  are used as observables. The precision on  $\xi$  is similar to that obtained in Section II B: since a comparable statistics has been used, we conclude that the benefit of dealing with a connected observable is not very significant.

### III. DETERMINATION OF $\lambda$ AND TYPOLOGY OF THE VACUUM

Several consistent determinations of the parameter  $\lambda$  can be found in the literature [5–10]: in this Section we will present an independent one obtained from the study of the flux tube profile between two static color charges.

We have analyzed, for two different values of the inverse gauge coupling,  $\beta = 2.5115$  and  $\beta = 2.6$ , the abelian projected flux tube formed between a quark and an antiquark placed at 16 lattice spacings apart from each other (corresponding respectively to 1.33 and 0.99 fm); the Maximal Abelian gauge has been chosen to define the abelian projection. In particular we have studied the correlation of the plaquette operator with a Wilson loop  $W(R, T)$  with  $R = 16$  and  $T = 6$ , on a lattice  $24 \times 24 \times 32 \times 24$ , with the longer dimension along the  $q\bar{q}$  axis. We adopt the following prescription for the electric field [10]:

$$E_i = \frac{\langle \text{tr} (W^{AbPr}(R, T) \Pi_{0i}^{AbPr}) \rangle}{\langle \text{tr} (W^{AbPr}(R, T)) \rangle} - \frac{\langle \text{tr} (W^{AbPr}(R, T)) \text{tr} \Pi_{0i}^{AbPr} \rangle}{2 \langle \text{tr} (W^{AbPr}(R, T)) \rangle}; \quad (3.1)$$

which is the definition satisfying the Maxwell equations on the lattice [10]. The flux tube profile has been studied at half a way between the two charges and at an equal temporal distance between the creation and annihilation times of the  $q\bar{q}$  pair. The Jackknife method for correlated quantities [26] has been used in the statistical analysis.

Having chosen a quite long flux tube, noise reduction is a critical point of our computation: we have adopted a standard cooling procedure, looking for a stable plateau in  $\lambda$  as a function of the cooling steps performed.

We have fitted our data according to the solution  $E_z = AK_0(\frac{d}{\lambda})$  of London equation  $\nabla^2 E_z = \frac{1}{\lambda^2} E_z$ : since that is expected to be valid beyond a certain distance  $d$  from the flux tube axis, where the effects of the non superconductive core are absent, we look for a plateau of  $\hat{\lambda}$  with respect to the minimum distance  $d_0$  included in the fit.

In figure 5 we report the dependence of  $\hat{\lambda}$  measured at  $\beta = 2.6$  both as a function of the fit starting point  $d_0$  at a fixed number of cooling steps ( $N_{cool} = 6$ ) and as a function of the number of cooling steps at a fixed fit starting point ( $d_0 = 3$ ). A plateau is visible in both cases and we choose  $d_0 = 3$  and 6 cooling steps as a reference.

Our fitted value at  $\beta = 2.6$  (Fig. 4, left) is  $\hat{\lambda}(\beta = 2.6) = 2.58 \pm 0.12$ ; a similar analysis at  $\beta = 2.5115$  (Fig. 4, right) leads to  $\hat{\lambda}(\beta = 2.5115) = 1.96 \pm 0.08$ . Converting our results into physical units (see Section II B) we obtain  $\lambda = 0.163 \pm 0.007$  fm at  $\beta = 2.5115$  and  $\lambda = 0.160 \pm 0.007$  fm at  $\beta = 2.6$  lattice in good agreement with previous literature (as one of the latest determinations we report  $\lambda = 0.157 \pm 0.003$  from Ref. [10]).

In Fig. 6 we report a summary of the results obtained for  $\lambda$  and  $\xi$  at the different values of the lattice spacing. While apparently  $\xi$  is consistently lower than  $\lambda$ , it is anyway clear that the two quantities are comparable, in agreement with the findings of previous

literature [7,8,10,11]. Our conclusion is therefore that the vacuum type of pure gauge QCD with two colors is close to the type I - type II boundary, even if marginally of type II.

Our result can be further clarified by looking for observable consequences of the QCD vacuum being a type I or type II superconductor: that will be the subject of next Section.

#### IV. ANALYSIS OF FLUX TUBES INTERACTIONS

Another direct (but qualitative) method to identify the typology of the vacuum is to look at the behavior of two close parallel flux tubes: in a type II superconductor nearby flux tubes repel each other, while attraction is expected for a type I superconductor.

We have looked at the flux tubes of two  $q\bar{q}$  pairs placed with their axes parallel to each other (and along the  $z$  direction). We have performed two simulations at  $\beta = 2.6$ , placing each quark at a distance of 16 lattice spacings from the respective antiquark and considering two different distances  $D$  between the two parallel  $q\bar{q}$  axes,  $D = 4$  and  $D = 5$ ; the lattice chosen is again a  $24 \times 24 \times 32 \times 24$  and following Section III, we have determined the abelian electric field in presence of two parallel Wilson loops  $W_1(R, T)$  and  $W_2(R, T)$  at distance  $D = 4a$  or  $D = 5a$ , with  $R = 16$  and  $T = 6$ . The quantity we look at is

$$E_i = \frac{\langle \text{tr} \left( W_1^{AbPr}(R, T) W_2^{AbPr}(R, T) \prod_{0i}^{AbPr} \right) \rangle}{\langle \text{tr} \left( W_1^{AbPr}(R, T) W_2^{AbPr}(R, T) \right) \rangle} - \frac{\langle \text{tr} \left( W_1^{AbPr}(R, T) W_2^{AbPr}(R, T) \right) \text{tr} \prod_{0i}^{AbPr} \rangle}{2 \langle \text{tr} \left( W_1^{AbPr}(R, T) W_2^{AbPr}(R, T) \right) \rangle} \quad (4.1)$$

that is the generalization of Eq. (3.1) satisfying the Maxwell equations on the lattice. Our statistics consist of about  $6 \cdot 10^4$  decorrelated configurations for each simulation.

We focus on the longitudinal  $E_z$  component in the  $xz$  plane reported in Fig. 7 where errors on  $E_z$  are of the order of 5% for almost all points. As in Section III we have used cooling for noise reduction: all data showed have been obtained after 6 cooling steps.

No evident repulsive or attractive behaviour can be appreciated from Fig. 7, however we have tried a quantitative analysis of flux tube deflection by measuring the average distance between the two tubes and comparing it with the distance  $D$  between the two  $q\bar{q}$  axes. The average distance has been taken over the central part of the flux tubes, including 9 lattice sites for each tube. We have defined the position of the flux tube in two different ways: first by the position of the local maximum for  $E_z$ , secondly by the weighted average position over the three lattice sites closest to the  $q\bar{q}$  axis, using  $E_z$  as a weight. We call the two definitions  $d_M$  and  $d_W$  respectively.

In Table III we report the data obtained for the deflections  $(d_M - D)$  and  $(d_W - D)$  as a function of  $D$ : a positive/negative value corresponds to a repulsive/attractive behaviour. While deflections are nearly compatible with zero at  $D = 5$ , some signal appears when the flux tubes are closer to each other, at  $D = 4$ . Although we have no clear sign of flux tube repulsion, we consider this as an important hint in that direction, even more if we consider that the superposition of the two flux tubes in the central region should bias our result in the opposite direction, leading to negative values of  $(d_M - D)$  and  $(d_W - D)$ .

In Section III we concluded that the vacuum is close to the type I - type II boundary, even if marginally on the type II side: that would imply a weak repulsive interaction between parallel flux tubes. That is consistent with the result of the present Section, *i.e.* that there are signs of weak repulsive interaction as the distance between the two flux tubes is

decreased. The still large uncertainties as well as the finite lattice spacing place a limit on the observable flux tube deflection. While the aim of the study presented in this Section was only to look for a possible evident signal of flux tube deformation, more refined investigations can be done, including a detailed analysis of Wilson loop interactions and a quantitative comparison with the determinations of  $\xi$  and  $\lambda$ , after also taking properly into account the quantum fluctuations of the flux tube. That is beyond the purpose of the present study and will be the subject of future investigations.

## V. CONCLUSIONS

The aim of our study was that of understanding which type of dual superconductor is realized in the vacuum of  $SU(2)$  pure gauge theory. We have followed two different strategies: a numerical determination of the parameters  $\xi$  and  $\lambda$  and an analysis of the interaction between parallel flux tubes.

To determine  $\xi$  we have studied the temporal correlator of an operator  $\mu$  which creates a magnetic monopole and whose vacuum expectation value has been shown to be an order parameter for dual superconductivity both in quenched and in full QCD. The greatest difficulty in our measurement derives from the necessity of isolating an exponentially decaying signal from a large background: that is why a very high precision is needed and numerical strategies such as analytic link integration have been used. We have determined  $\xi$  for four different values of the inverse coupling  $\beta$  and, in some cases, for different lattice volumes and for different charges  $Q$  of the magnetic monopole. We have explicitly checked that our results are independent of the abelian projection used to define  $\mu$ , that they have no significant dependence on the monopole charge  $Q$  and that they are not affected by finite volume effects within our statistical uncertainties. Data are compatible within errors with the correct scaling to the continuum limit, even if a reliable extrapolation to that limit cannot still be performed. Results are summarized in Table II and our estimate for the correlation length, based on the determination at the largest value of  $\beta$ , is  $\xi = 0.11 \pm 0.02$  fm. We have also repeated our measurement using an alternative way to study the temporal correlator [21], obtaining a good agreement. We would like to stress the consistency of our results with those reported in Ref. [11], which were obtained through a completely different method, consisting in the study of the correlations of monopole currents around the flux tube.

To determine  $\lambda$  we employed the usual analysis of the longitudinal component of the abelian chromoelectric field inside the flux tube. We performed our measurement at two different couplings,  $\beta = 2.5115$  ( $\lambda = 0.163(7)$  fm) and  $\beta = 2.6$  ( $\lambda = 0.160(7)$  fm), obtaining a good agreement with previous literature.

Our determinations show that  $\xi$  is smaller than  $\lambda$ , even if comparable to it in magnitude: this indicates that the vacuum of pure gauge QCD with two colors is close to the type I - type II boundary and marginally of type II. This is consistent with our direct investigation presented in Section IV, showing some weak signals of repulsive interactions as two parallel flux tubes are brought closer to each other.

One way to improve our results would be to make a more precise determination of  $\xi$ : the great noise in the signal obtained for the temporal correlator has been a limitation and no significant improvement has been achieved when adopting the alternative approach

proposed in Ref. [21]. One reason for the problems encountered can be traced back to the small value of  $\xi$  itself ( $\xi \sim 0.1$  fm), which makes the signal to fade away very rapidly after a few lattice spacings. One possible strategy to overcome this limitation could be to make use of anisotropic lattices with a very small lattice spacing in the temporal direction; we will also consider direct determinations of the correlator  $\langle \bar{\mu}(t, \vec{x}) \mu(0, \vec{x}) \rangle$ , in place of its derivatives  $\rho(t)$  or  $\tilde{\rho}(t)$ , using a technique recently developed for the  $U(1)$  gauge theory [27]. Finally, a more refined investigation of flux tube interactions could be performed, using also finer lattice spacings in order to be more sensitive to small flux tube deflections.

As an extension of our study, we will repeat in the future the determination of  $\xi$  also around or slightly above the deconfinement critical temperature  $T_c$ , where  $\xi$  could be directly related to the mass of physical magnetic monopoles: that could be quite relevant from a phenomenological point of view, if the hypothesis [28] of light monopole degrees of freedom populating the quark gluon plasma slightly above the transition is correct. Of course it would be also of fundamental importance to extend our investigation to the case of pure gauge theory with 3 colors and eventually to full QCD.

### ACKNOWLEDGEMENTS

It is a pleasure to thank A. Di Giacomo for useful comments and discussions. Numerical simulations have been run on two PC farms at INFN - Genova and at CNAF - Bologna. This work has been partially supported by MIUR.

## REFERENCES

- [1] G. 't Hooft, in “High Energy Physics”, EPS International Conference, Palermo 1975, ed. A. Zichichi.
- [2] S. Mandelstam, Phys. Rept. **23**, 245 (1976).
- [3] G. Parisi, Phys. Lett. **B60**, 93 (1975)
- [4] G. 't Hooft, Nucl. Phys. **B190**, 455 (1981).
- [5] Y. Matsubara, S. Ejiri, T. Suzuki, Nucl. Phys. B (Proc. Suppl.) **34**, 176 (1994).
- [6] P. Cea and L. Cosmai, Phys. Rev. **D52**, 5152 (1995).
- [7] G. S. Bali, C. Schlichter, K. Schilling, Prog. Theor. Phys. Suppl. **131** 645 (1998) 645.
- [8] F. V. Gubarev, E. M. Ilgenfritz, M. I. Polikarpov, T. Suzuki, Phys. Lett. B **468** 134 (1999).
- [9] Y. Koma, M. Koma, E. M. Ilgenfritz, T. Suzuki, Phys. Rev. D **68**, 114504 (2003).
- [10] R. W. Haymaker and T. Matsuki, arXiv:hep-lat/0505019.
- [11] M. N. Chernodub *et al.*, Phys. Rev. D **72**, 074505 (2005); T. Sekido, K. Ishiguro, Y. Mori and T. Suzuki, arXiv:hep-lat/0703003.
- [12] A. Di Giacomo and G. Paffuti, Phys. Rev. D **56**, 6816 (1997).
- [13] J. Fröhlich and P.A. Marchetti, Phys. Rev. D **64**, 014505 (2001)
- [14] P. Cea and L. Cosmai, Phys. Rev. D **62**, 094510 (2000); P. Cea, L. Cosmai, M. D’Elia, JHEP 02, 018 (2004).
- [15] A. Di Giacomo, B. Lucini, L. Montesi, G. Paffuti, Phys. Rev. D **61**, 034503 (2000).
- [16] A. Di Giacomo, B. Lucini, L. Montesi, G. Paffuti, Phys. Rev. D **61**, 034504 (2000).
- [17] J. M. Carmona, M. D’Elia, A. Di Giacomo, B. Lucini, G. Paffuti, Phys. Rev. D **64**, 114507 (2001).
- [18] J.M. Carmona, M. D’Elia, L. Del Debbio, A. Di Giacomo, B. Lucini, G. Paffuti, Phys. Rev. D **66**, 011503 (2002)
- [19] M. D’Elia, A. Di Giacomo, B. Lucini, G. Paffuti, C. Pica, Phys. Rev. D **71**, 114502 (2005).
- [20] A. D’Alessandro and M. D’Elia, arXiv:hep-lat/0510112.
- [21] L. Tagliacozzo, Phys. Lett. B **642**, 279 (2006).
- [22] J. Fingberg, U. M. Heller and F. Karsch, Nucl. Phys. **B 392**, 493 (1993).
- [23] J. Engels, F. Karsch and K. Redlich, Nucl. Phys. **B 435**, 295 (1995).
- [24] A. Di Giacomo, hep-lat/0206018; A. Di Giacomo, G. Paffuti, Nucl. Phys. (Proc.Suppl.) **129**, 647 (2004).
- [25] P. Majumdar, Y. Koma and M. Koma, Nucl. Phys. **B 677**, 273 (2004).
- [26] H. Flyvbjerg, H. G. Petersen J. Chem. Phys. **91**, 461 (1989)
- [27] M. D’Elia and L. Tagliacozzo, Phys. Rev. D **74**, 114510 (2006).
- [28] M. N. Chernodub and V. I. Zakharov, arXiv:hep-ph/0611228.

TABLES

	$\hat{t}_0 = 1$	$\hat{t}_0 = 2$	$\hat{t}_0 = 3$	$\hat{t}_0 = 4$	$\hat{t}_0 = 5$
$12^3 \times 16, \beta = 2.4, Q = 2$	$0.857 \pm 0.021$	$1.07 \pm 0.07$	$1.02 \pm 0.20$	$4.5 \pm 3.8$	
$12^3 \times 20, \beta = 2.5115, Q = 2$		$1.28 \pm 0.08$	$1.36 \pm 0.21$	$1.8 \pm 1.5$	
$16^3 \times 20, \beta = 2.5115, Q = 2$	$0.99 \pm 0.03$	$1.14 \pm 0.10$	$1.28 \pm 0.25$	$1.0 \pm 0.4$	
$20^3 \times 20, \beta = 2.6, Q = 2$	$1.24 \pm 0.03$	$1.33 \pm 0.05$	$1.52 \pm 0.17$	$3.6 \pm 1.5$	
$20^3 \times 20, \beta = 2.6, Q = 8$	$1.06 \pm 0.03$	$1.32 \pm 0.08$	$1.62 \pm 0.23$	$1.8 \pm 0.6$	$1.2 \pm 1.0$
$20^3 \times 20, \beta = 2.7, Q = 8$	$1.34 \pm 0.02$	$1.51 \pm 0.04$	$1.78 \pm 0.11$	$2.4 \pm 0.4$	$1.7 \pm 0.8$

TABLE I. Dependence of  $\hat{\xi}$  on the fit starting point  $\hat{t}_0$  for our sets of numerical simulations (fit according to Eq. 2.10).

$\beta$	$a(\beta)$	$\xi$
2.4	0.118 fm	$0.126 \pm 0.008$ fm
2.5115	0.083 fm	$0.106 \pm 0.021$ fm
2.6	0.062 fm	$0.094 \pm 0.011$ fm ( $Q = 2$ ), $0.100 \pm 0.014$ fm ( $Q = 8$ )
2.7	0.046 fm	$0.110 \pm 0.018$ fm

TABLE II. Lattice spacing  $a$  and correlation length  $\xi$  for different values of  $\beta$ .

$D$	$d_M - D$	$d_W - D$
4	0.44(17)	0.017(9)
5	0.22(14)	-0.007(15)

TABLE III. Average deflection (in lattice spacing units) at  $\beta = 2.6$  for two parallel flux tubes as a function of the distance  $D$  between the  $q\bar{q}$  axes. See text for the definition of  $d_M$  and  $d_W$ .

FIGURES

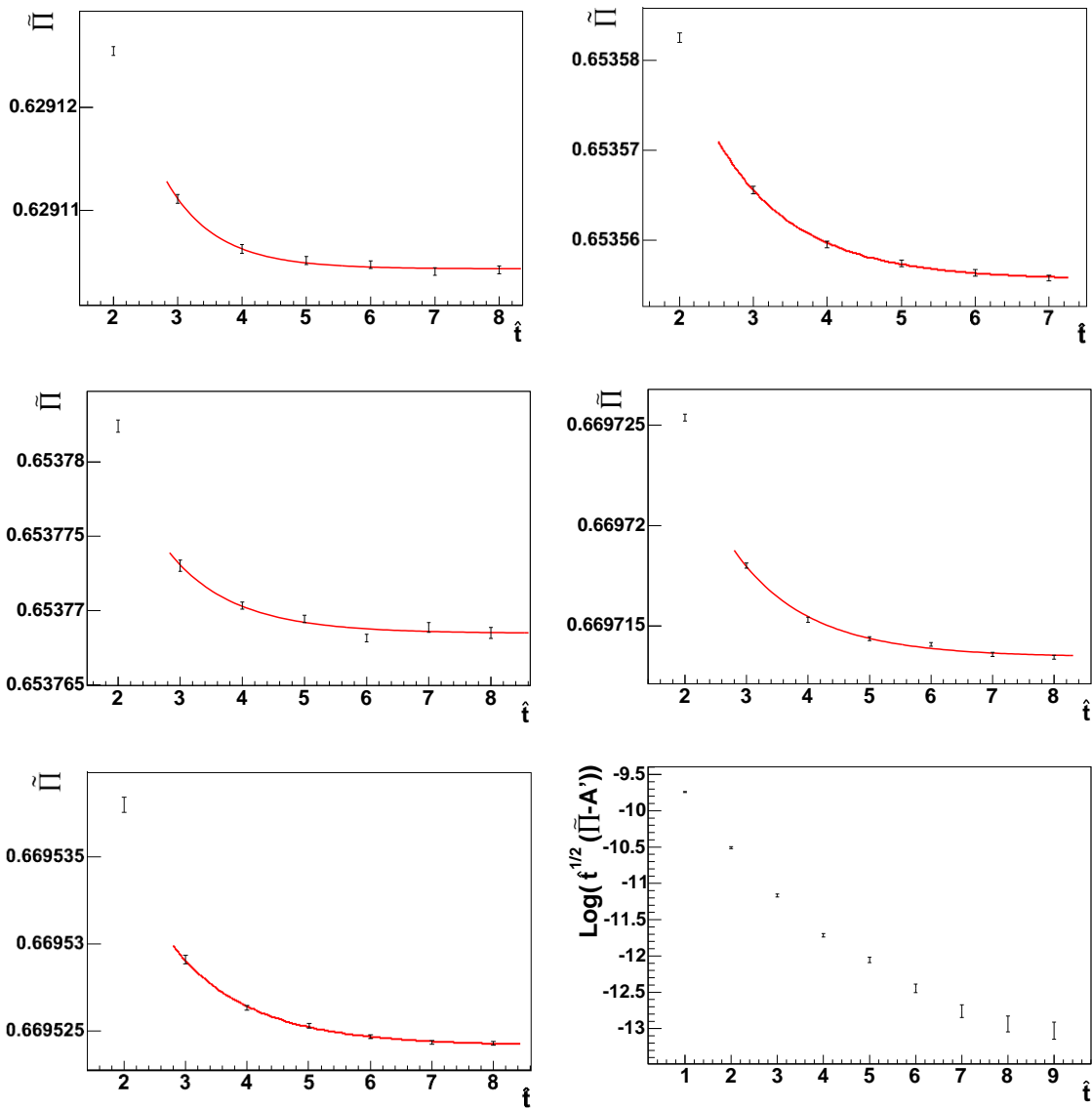


FIG. 1. Modified average plaquette as a function of  $\hat{t}$  for a  $12^3 \times 16$  lattice at  $\beta = 2.4$  (top left), a  $12^3 \times 20$  lattice at  $\beta = 2.5115$  (top right), a  $16^3 \times 20$  lattice at  $\beta = 2.5115$  (middle left), a  $20^3 \times 20$  lattice at  $\beta = 2.6$  with  $Q = 2$  (middle right), a  $20^3 \times 20$  lattice at  $\beta = 2.6$  with  $Q = 8$  (bottom left) and a  $20^3 \times 20$  lattice at  $\beta = 2.7$  with  $Q = 8$  (bottom right). In the last case ( $\beta = 2.7$ ) we have actually plotted the quantity  $\log(\hat{t}^{1/2}(\tilde{\Pi} - A))$  (see Eq. (2.10)) in order to highlight the physical signal in the correlator.

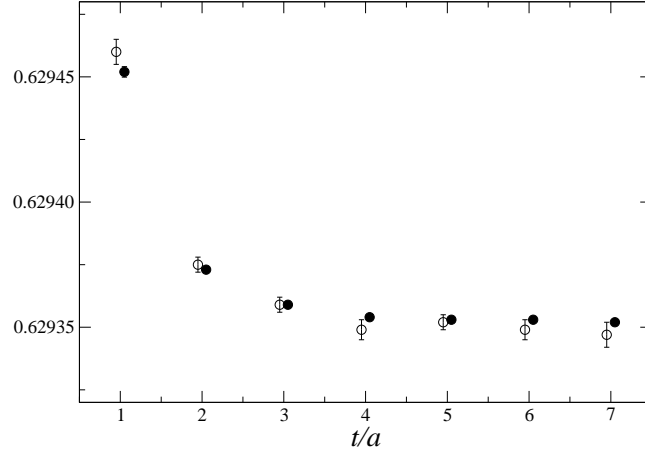


FIG. 2. Mean modified plaquette in the random gauge and in the Polyakov gauge: an offset has been added in order to compare the two sets of data, which lead to compatible correlation lengths.

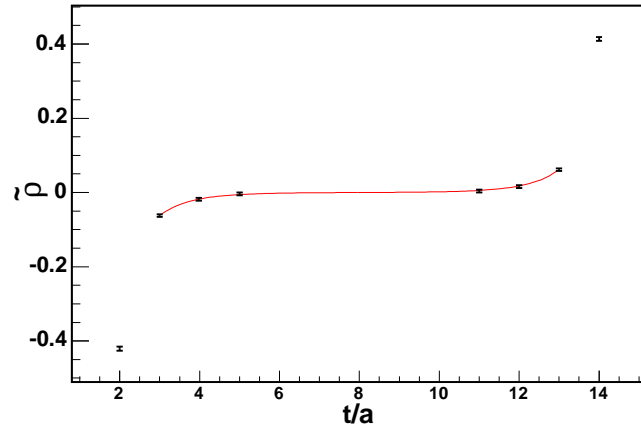


FIG. 3. Parameter  $\tilde{\rho}$  measured at  $\beta = 2.5115$  on a  $12^3 \times 16$  lattice.

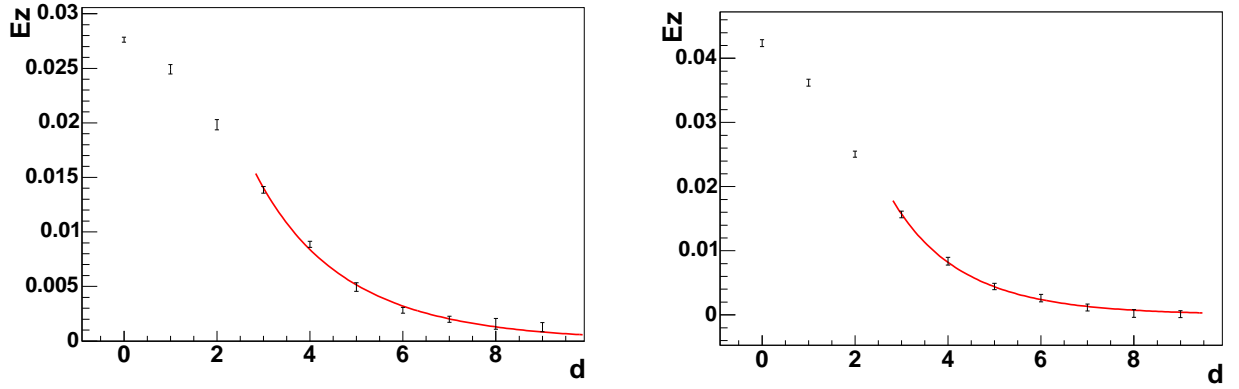


FIG. 4. Profile of  $E_z$  after 6 cooling steps for a  $24 \times 24 \times 32 \times 24$  lattice at  $\beta = 2.6$  (left) and at  $\beta = 2.5115$  (right). The black line refers to a fit with the function  $AK_0(\frac{d}{\lambda})$ .

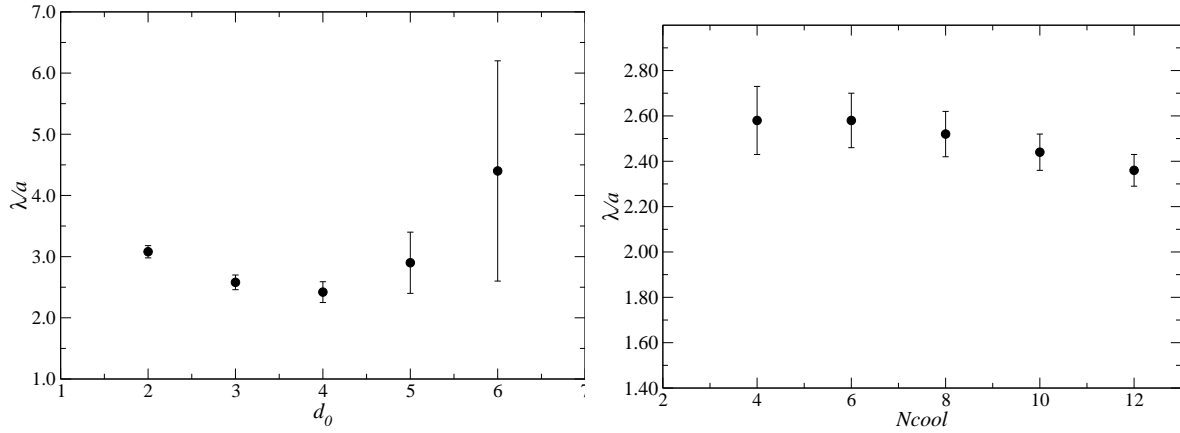


FIG. 5.  $\hat{\lambda}$  as a function of the fit starting point  $d$  (left) and as a function of the number of cooling steps (right) at  $\beta = 2.6$ .

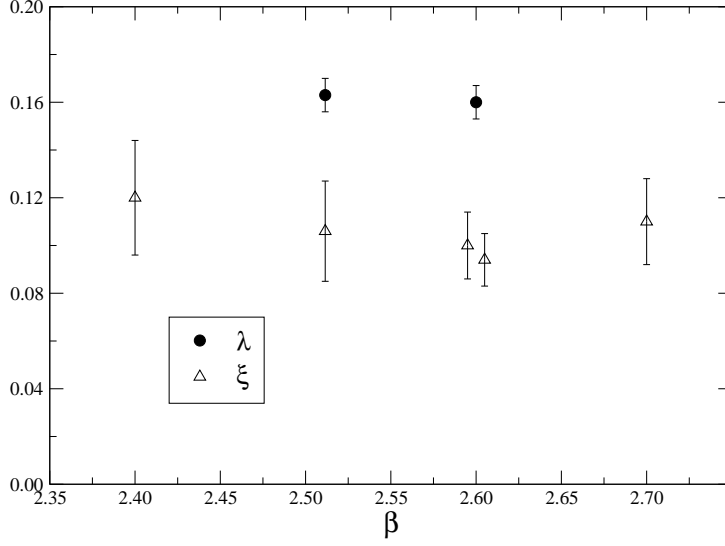


FIG. 6.  $\xi$  and  $\lambda$  in fermi units for different values of  $\beta$ . The two different values shown at  $\beta = 2.6$ , which have been slightly split apart for the sake of clarity, correspond to two different monopole charges,  $Q = 8$  and  $Q = 2$  respectively.

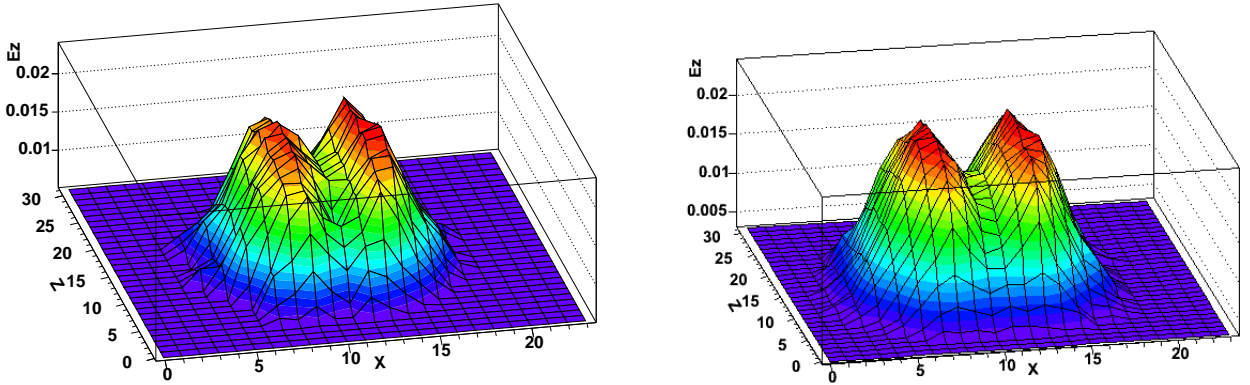


FIG. 7. Profile of the two interacting flux tubes on the  $xz$  plane placed at different relative distances ( $D = 4$  and  $D = 5$ ): the two  $q\bar{q}$  axes are placed respectively at  $x = 9$  and  $x = 13$  (left), and at  $x = 8$  and  $x = 13$  (right). The electric field has been measured after 6 cooling steps.